



# Morphology control of noble metal catalysts from planar to dendritic shapes by galvanic displacement

Seungyeon Baek<sup>a</sup>, Kwang Hwan Kim<sup>a</sup>, Myung Jun Kim<sup>b,\*</sup>, Jae Jeong Kim<sup>a,\*</sup>

<sup>a</sup> School of Chemical and Biological Engineering, Institute of Chemical Process, Seoul National University, 1 Gwanak-ro, Gwanak-gu, Seoul 08826, Republic of Korea

<sup>b</sup> Department of Chemistry, Duke University, 124 Science Drive, Box 90354, Durham, NC 27708, United States



## ARTICLE INFO

### Article history:

Received 9 February 2017

Received in revised form 25 April 2017

Accepted 31 May 2017

Available online 3 June 2017

### Keywords:

Galvanic displacement

Noble metal catalyst

Whisker structure

Electrochemical analysis

Ethanol oxidation

## ABSTRACT

Noble metal electrocatalysts can simply be prepared via galvanic displacement method on a sacrificial substrate, which is advantageous for preparing a uniform and thin catalyst layer. However, it is difficult to control the morphology of deposited metals via galvanic displacement, therefore, there is a limitation to increase the surface area of electrocatalysts. In this study, we demonstrate galvanic displacement for controlling the morphology of Pd, Pt, and Au from planar to whisker shapes by manipulating the dissolution rate of the sacrificial Cu substrate and the mass transport of noble metal ions. The acceleration of the dissolution of sacrificial substrate increases the reduction rate of noble metal, which develops a steep concentration gradient of noble metal ions near the surface of substrate. This induces the selective deposition of noble metal to form a whisker instead of smooth film. To verify the advantage of whisker-type catalysts, the ethanol oxidation with Pd is investigated. Whisker-type Pd shows 21 times higher electrocatalytic performance than planar Pd due to larger surface area. Therefore, it can be suggested that whisker-type catalysts simply prepared by galvanic displacement is applicable for various electrocatalytic reactions.

© 2017 Elsevier B.V. All rights reserved.

## 1. Introduction

The rational design of noble metal catalysts such as Pd, Pt, and Au is of considerable interest because of their superior properties in a number of applications including catalysts, electronics, sensing, photonics, imaging, and biomedicine [1]. Although noble metals are promising catalysts, their high cost represents an obstacle to commercialization [2]. Therefore, extensive studies have focused on improvement of their catalytic activity with a small loading amount by modifying their morphology or controlling their electronic structure. Coating of a substrate with a catalyst of high surface area-to-volume ratio – such as nanoparticles [3], nanowires [4], hollow or porous structures [5,6] – results in enhanced activity due to the dramatically increased surface area. Changes in the d-band center, determined by the alloy composition or the underlying substrate coated by the catalyst, also increase the catalytic performance [7,8].

Catalysts with a large surface area exhibit high catalytic activity due to their high concentration of the active sites for the electrochemical reactions [9]. As mentioned above, the substrate-

mediated preparation is one of the most common techniques of fabricating the extended-surface catalysts. A 3D-structured substrate consisting of comparably inexpensive material can be prepared using the anodization method [10], polyol method [11], or hard or soft substrate method [12,13] prior to coating of the catalyst film on the substrate. Noble metal catalysts are then coated on the prepared substrates by galvanic displacement [14–16], electroless deposition [17,18], and electrodeposition [19,20]. However, electroless deposition has several disadvantages, as it is a complex system involving use of various organics in the solution, which makes examination of the deposition characteristics problematic [21]. Furthermore, electrodeposition requires electrical energy for the process and limits the substrates to only conductive materials with low electrical resistance [22]. In contrast, catalyst deposition using galvanic displacement is a facile and economically sustainable method of spontaneous deposition that requires no additional energy supply; deposition occurs simply by immersing a substrate in the solution containing the ionic precursors of metal to be deposited [23,24]. Galvanic displacement is mediated by the difference in standard reduction potentials; the metal substrate is spontaneously oxidized upon coming into contact with an ionized metal source with a more positive reduction potential. The electrons generated from the oxidation reaction, i.e. dissolution of the

\* Corresponding authors.

E-mail addresses: [kmj4717@gmail.com](mailto:kmj4717@gmail.com) (M.J. Kim), [jjkimm@snu.ac.kr](mailto:jjkimm@snu.ac.kr) (J.J. Kim).

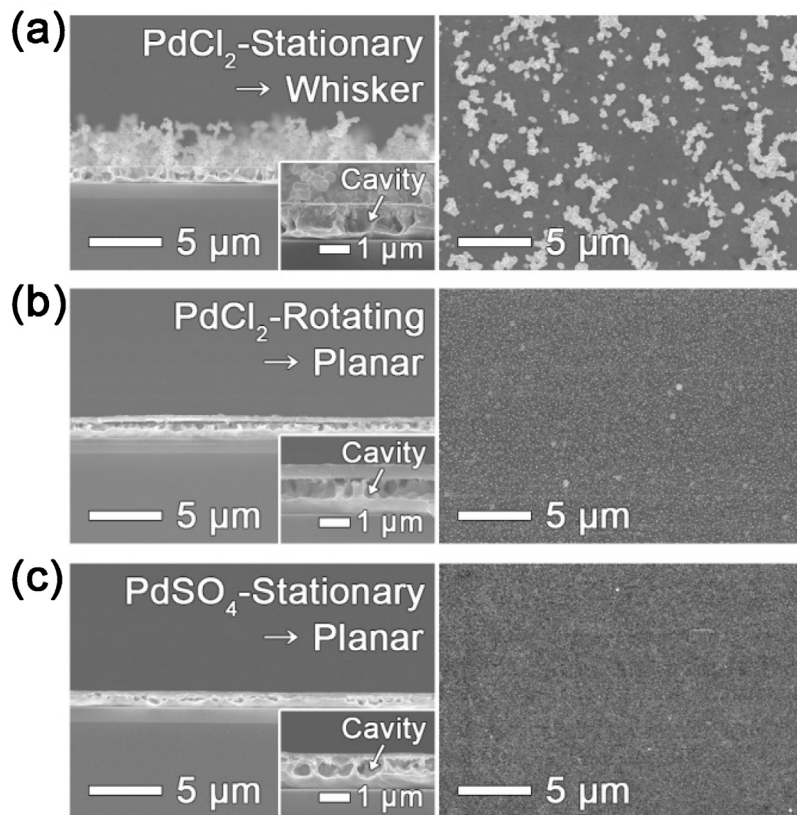


**Fig. 1.** Surface and cross-sectional images of Pd deposits prepared by galvanic displacement reaction (a, b) in the  $\text{PdCl}_2$  solution and (c) in the  $\text{PdSO}_4$  solution. The substrate remained (a, c) stationary for 30 min or (b) rotating at 300 rpm for 2 min during the reaction.

substrate, go towards the reduction reaction, i.e. metal deposition on the substrate.

The metal deposition via galvanic displacement reaction consists of nucleation and growth steps. Nucleated metal particles on the surface at the initial stage of the reaction grow until fully covering the substrate, which generally results in two-dimensional films [25–28]. Therefore, it is hard to control the morphology or increase the surface area via simple galvanic displacement method alone. If one-pot synthesis of catalysts with a large surface area using galvanic displacement from the planar sacrificial substrate can be developed, it can simplify the preparation procedures of electrocatalysts for various electrochemical reactions. Furthermore, the enlargement of surface area can dramatically enhance the electrocatalytic performance of metal deposits.

In this study, we introduced a one-step synthetic approach to synthesis of a whisker catalyst on a flat Cu substrate by galvanic displacement. Mechanistic analyses of Pd whisker formation are presented to elucidate the effects of the mass transport of metal cation and the oxidation rate of the sacrificial Cu substrate on the morphology of metal deposits. We proposed a universal mechanism of controlling the morphology of noble metal (Pd, Pt, and Au) catalysts; i.e., whisker or smooth film prepared via galvanic displacement. Furthermore, Pd-based whisker catalyst for ethanol oxidation was investigated to present the advantages of whisker-type electrocatalysts.

## 2. Experimental

### 2.1. Sample preparation

Pd-based catalyst was synthesized simply by dipping Cu substrate in an aqueous solutions containing 0.1 M  $\text{HClO}_4$  (70%, Junsei)

and 3 mM  $\text{PdCl}_2$  (99%, KOJIMA) or 3 mM  $\text{PdSO}_4$  (99%, Alfa Aesar). A Cu coupon wafer, whose structure was Cu (PVD, 1  $\mu\text{m}$ )/TaN (PVD, 30 nm)/Ta (PVD, 30 nm)/TaN (PVD, 30 nm)/ $\text{SiO}_2$ /Si, was used as the sacrificial substrate. Before the galvanic displacement reaction, the Cu substrate was immersed in an aqueous solution of 20.4 mM citric acid (99.5%, Sigma Aldrich) and 35.6 mM KOH (95%, SAMCHUN) for 2 min to eliminate the native Cu oxide. The pretreated wafer was rinsed in deionized water, followed by immersion in the displacement bath. Galvanic displacement was conducted with stationary or 300 rpm-rotating substrate at 25 °C.  $\text{K}_2\text{PtCl}_4$  (99.99%, Sigma Aldrich) or  $\text{AuCl}_3$  (99.999%, Sigma Aldrich) (each 3 mM) was also used as a precursor for the Pt and Au displacement, respectively.

### 2.2. Electrochemical analyses

All electrochemical experiment was conducted in a three-electrode system containing Pt wire as a counter electrode and saturated calomel electrode (SCE) as a reference electrode. The effect of counter anions in Pd precursors,  $\text{Cl}^-$  and  $\text{SO}_4^{2-}$ , on the kinetics of the oxidation reaction (i.e. dissolution of Cu substrate) was examined by comparing exchange current densities obtained from Tafel plot with a Cu rotating disk electrode (RDE,  $A=0.196 \text{ cm}^2$ ) as a working electrode in (i) 6 mM KCl, 0.1 M  $\text{HClO}_4$  and (ii) 3 mM  $\text{K}_2\text{SO}_4$ , 0.1 M  $\text{HClO}_4$  aqueous solutions. Furthermore, cyclic voltammetry was carried out to estimate the diffusion coefficient of the Pd complex with a glassy carbon electrode ( $A=0.196 \text{ cm}^2$ ). The scan rate for cyclic voltammetry was between 10 and 100  $\text{mV s}^{-1}$ . In addition, the electrochemically active surface area of Pd disk ( $A=0.196 \text{ cm}^2$ ) and whisker electrodes was analyzed by cyclic voltammetry in 0.5 M KOH aqueous solution. Pd disk electrode was polished carefully with 0.3 and 0.05  $\mu\text{m}$  alumina powders, and it was rinsed by deionized water with ultrasoni-

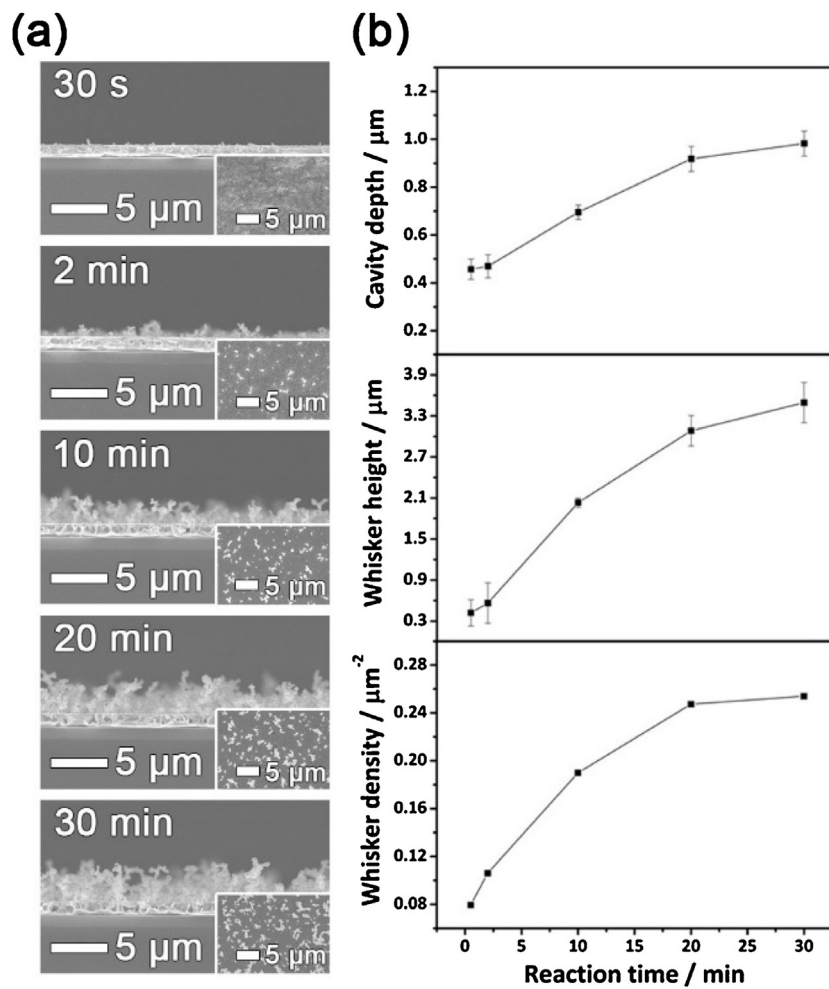


**Fig. 2.** (a) Surface and cross-sectional images of Pd deposits after galvanic displacement in  $\text{PdCl}_2$  solution without forced convection and (b) the changes in the cavity depth, whisker height and density according to the reaction time.

cation after each mechanical polishing step. The electrocatalytic activity of whisker and Pd disk for the ethanol oxidation reaction was measured by cyclic voltammetry in an aqueous solution containing 1 M KOH and 1 M ethanol (EtOH; 94.5%, DAEJUNG). The scan rate of cyclic voltammetry was  $20 \text{ mV s}^{-1}$ . Before each measurement, the electrodes were electrochemically pretreated by repeating the cyclic voltammetry to obtain the reproducible electrochemical measurements. The long-term stability of electrodes for ethanol oxidation reaction was investigated by a chronoamperometry performed at  $-0.245 \text{ V}$  for 3600 s. The aforementioned electrochemical analyses for ethanol oxidation were conducted with 1600 rpm-rotating working electrodes at  $25^\circ\text{C}$  and using a potentiostat (VersaStatII, EG&G).

### 2.3. Characterization of metal deposits

The surface and cross-sectional morphologies of the prepared catalyst were examined by field emission-scanning electron microscopy (FE-SEM; S-4800, Hitachi). The composition of the metal deposit was analyzed by transmission electron microscopy (TEM; JEM-2100F, JEOL) and energy-dispersive X-ray spectroscopy (EDS; INCA Energy, Oxford Instruments Analytical Ltd.). Crystal information was also obtained using an X-ray diffractometer (XRD; Bruker, D8-Advance). The amount of Pd deposited by galvanic displacement was measured by inductively coupled plasma-mass spectrometer (ICP-MS; Varian 820-MS, Varian). The atomic ratio in planar layers was calculated from the peak intensities measured by

X-ray photoelectron spectroscopy (XPS; K-Alpha, Thermo Electron) [29,30]. The method to calculate the atomic ratio is introduced in Supporting Information.

## 3. Results and discussion

### 3.1. Formation of whiskers via galvanic displacement

The dendritic growth of metal using electrodeposition has been achieved by depleting the metal ions near the surface with high reduction rate, i.e. under the mass-transfer limited condition. The metal ions transporting from the bulk electrolyte to the electrode surface are in turn reduced at the end of dendrite [31]. That is, the mass transport of metal ions and their concentration gradient during deposition can change the morphology of the metal deposit. In galvanic displacement, two electrochemical reactions take place: dissolution of the sacrificial substrate (oxidation reaction) and deposition of the noble metal (reduction reaction), and the rates of both reactions should be identical. Therefore, it is possible to control the morphology of metal deposit by modifying the rates of electrochemical reactions and mass transfer of noble metal ions, similar to the case of electrodeposition. The addition of  $\text{Cl}^-$  is one of the ways to change the rate of the electrochemical reaction because the dissolution of Cu can be accelerated by  $\text{Cl}^-$ , leading to an increase in the reduction rate of Pd. In addition, the mass transfer of metal ions can be modified: (i) by changing the diffusivity of Pd ions with modification of the complex between Pd ions and counter

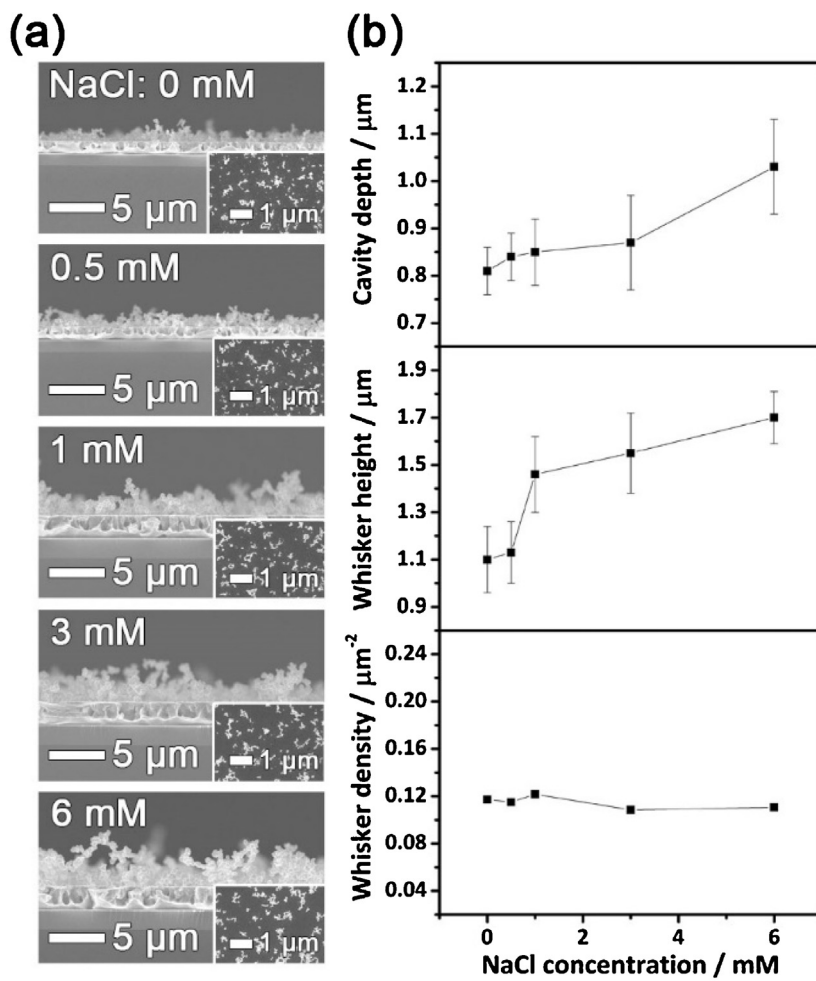


**Fig. 3.** (a) Surface and cross-sectional images of Pd deposits after galvanic displacement in  $\text{PdCl}_2$  solution with varying the concentration of  $\text{Cl}^-$  and (b) the changes in the cavity depth, whisker height and density. The reaction was performed without substrate rotation for 5 min.

anions and (ii) by simply rotating the substrate during the reaction. Therefore, we first investigated the effects of aforementioned variables on the morphology of Pd deposit.

The deposit morphologies according to Pd precursors and substrate rotation during the reaction are shown in Fig. 1. The rotation of Cu substrate was for promoting the mass transport of Pd ions, resulting in less development of a concentration gradient of Pd ions during the displacement reaction. Although the Cu substrates used in this study were smooth and free from defects (Fig. S1), cavities were formed in Cu substrate after the galvanic displacement, regardless of solution composition and substrate rotation. These cavities originated from severe dissolution of Cu during galvanic displacement. In contrast, the structure of deposited metal depended on the solution composition and substrate rotation. As indicated in Fig. 1(a), the height and density of whiskers prepared in  $\text{PdCl}_2$  solution without rotation were  $3.5 \mu\text{m}$  ( $\pm 0.3$ ) and  $0.254 \mu\text{m}^{-2}$  ( $\pm 0.011$ ), respectively. However, when the substrate rotated during the displacement reaction, a flat and smooth deposit with no whiskers was observed (Fig. 1(b)). Also, displacement in  $\text{PdSO}_4$  instead of  $\text{PdCl}_2$  solution resulted in formation of planar deposit even without substrate rotation (Fig. 1(c)). This suggested that  $\text{Cl}^-$  and the rotation of substrate (i.e. mass transport of Pd ions during the reaction) play a critical role to determine the final morphology of metal deposited by galvanic displacement.

To investigate changes in morphology over time, the reaction time was increased from 30 s to 30 min. Fig. 2(a) shows the changes

in the morphology of metal deposit according to the reaction time. The height and density of whiskers, and the depth of cavities measured from these images are presented in Fig. 2(b). At the initial stage of displacement reaction (30 s), the aggregated particles were formed with small cavities in Cu substrate. As the reaction proceeded, whiskers started to grow from the aggregated particles, and their height and density continuously increased. The morphological change of Pd deposits from  $\text{PdSO}_4$  solution is shown in Fig. S2, and the change in the cavity depth is presented in Fig. S3. Planar film was observed with gradual increases in both the thickness and the cavity in Cu substrate. Interestingly, the growth rate of cavity in  $\text{PdSO}_4$  solution was much lower than that in  $\text{PdCl}_2$  solution. Since the formation of cavities is originated from the anodic reaction of Cu, the reduction rate of Pd can be surmised from the size of cavities. Therefore, the reduction rate of Pd with  $\text{Cl}^-$  was found to be much faster than that with  $\text{SO}_4^{2-}$ . From Figs. 1 and 2, it can be suggested that the rate of galvanic displacement reaction was controlled by  $\text{Cl}^-$  and the substrate rotation promoting Pd ion diffusion affected the structure of Pd deposited by galvanic displacement. Therefore, the effect of  $\text{Cl}^-$  on the oxidation rate of Cu substrate and the diffusion of Pd complex was investigated in the aspect of the development of concentration gradient of Pd ions.

### 3.2. The mechanism of whisker formation

The formation of cavities resembled the pitting corrosion phenomenon in the presence of  $\text{Cl}^-$  reported by Otmačae et al. [32].

The effect of  $\text{Cl}^-$  on cavity depth and whisker height was examined by adding  $\text{NaCl}$  to the galvanic displacement bath (Fig. 3) because  $\text{Cl}^-$  can accelerate the dissolution of  $\text{Cu}$  by forming  $\text{CuCl}_2^-$  ions. The cavity depth and whisker height according to  $\text{NaCl}$  concentration on the substrates after 5 min of displacement reaction increased with the increasing  $\text{Cl}^-$  concentration although the density of whisker changed very little. This result indicates that  $\text{Cu}$  dissolution; i.e., the oxidation reaction during galvanic displacement, was accelerated by  $\text{Cl}^-$ , and resulted in huge cavities within the  $\text{Cu}$  substrate. This acceleration of oxidation reaction can promote the deposition of  $\text{Pd}$  which is the coupled reduction reaction in galvanic displacement. The accelerated consumption of  $\text{Pd}$  ion led to rapid development of concentration gradient of  $\text{Pd}$  ions, which enhanced vertical growth of  $\text{Pd}$  because  $\text{Pd}$  is more readily deposited at the end of whiskers than at the side or on substrate. This was supported by the height of whisker increased with higher concentration of  $\text{Cl}^-$  at the same reaction time.

As depicted in Fig. 1(c), the film-type  $\text{Pd}$  from  $\text{PdSO}_4$  solution also shows the formation of cavities in the  $\text{Cu}$  substrate, although the size of cavities was smaller than that formed with  $\text{Cl}^-$ . It can be expected from the size of cavities that the reduction rate of  $\text{Pd}$  with  $\text{Cl}^-$  was much faster than with  $\text{SO}_4^{2-}$ . However, the comparison of the dissolution rate according to  $\text{Cl}^-$  and  $\text{SO}_4^{2-}$  is required to verify the assumption that the change in the cavity size is matched to the rates of  $\text{Cu}$  oxidation and  $\text{Pd}$  reduction. To quantitatively compare the kinetics of  $\text{Cu}$  dissolution with  $\text{Cl}^-$  and  $\text{SO}_4^{2-}$ , the exchange current densities for  $\text{Cu}$  pitting corrosion in  $\text{KCl}$  and  $\text{K}_2\text{SO}_4$  solutions were measured using a Tafel plot (Fig. 4(a)) to be 2.34 and 2.01  $\text{mA cm}^{-2}$ , respectively, which are with a standard deviation of 0.01  $\text{mA cm}^{-2}$ . The kinetics of  $\text{Cu}$  corrosion with  $\text{Cl}^-$  was 1.16-fold faster than that with  $\text{SO}_4^{2-}$ . That is, the acceleration effect of  $\text{Cl}^-$  on  $\text{Cu}$  oxidation helped the development of  $\text{Pd}$  concentration gradient near the substrate surface by providing more electrons to  $\text{Pd}$  ions for their reductions.

As mentioned above, the complex between  $\text{Pd}$  ions and anions changes the mass transfer rate of  $\text{Pd}$  ion from the bulk solution to the substrate surface, and this might also have additional effect on whisker formation. If the  $\text{Pd}$  ion in coordination with  $\text{Cl}^-$  has lower diffusivity, the effect of corrosion rate on the development of concentration gradient of  $\text{Pd}$  ion becomes more significant than the case with  $\text{SO}_4^{2-}$ . That is, the planar deposit can be obtained with more rapid diffusion of  $\text{Pd}$  complex by maintaining higher concentration of  $\text{Pd}$  at the substrate surface. Therefore, cyclic voltammetry was performed to determine the diffusion coefficients of  $\text{Pd}$  complexes with  $\text{Cl}^-$  and  $\text{SO}_4^{2-}$  (Fig. 4(b) and (c)). Diffusion coefficients of the  $\text{Pd}$  complexes from the  $\text{PdCl}_2$  and  $\text{PdSO}_4$  solutions were found to be  $1.36 \times 10^{-8} \text{ cm}^2 \text{ s}^{-1}$  and  $4.59 \times 10^{-8} \text{ cm}^2 \text{ s}^{-1}$ , respectively (calculation method shown in Supporting Information). The higher diffusion coefficient of  $\text{Pd-SO}_4$  complex resulted from weak coordination of the counter anion,  $\text{SO}_4^{2-}$  [33], which did not severely diminish the diffusion of  $\text{Pd}$  complex. On the contrary, the slow diffusion rate of  $\text{Pd-Cl}$  complex led to the relatively easy depletion of  $\text{Pd}$  ions near the surface (i.e. the formation of a large concentration gradient of  $\text{Pd}$  ions during displacement).

The mechanism for whisker formation during galvanic displacement is summarized in Fig. 5.  $\text{Cl}^-$  accelerates the oxidation reaction of  $\text{Cu}$  which promotes the reduction reaction of noble metal ions. Furthermore, the diffusion of the complex between metal ion and  $\text{Cl}^-$  ions is slower than that of  $\text{SO}_4^{2-}$ -complex. Therefore, the steep concentration gradient is developed with  $\text{Cl}^-$  ion during the galvanic displacement reaction, and the reduction reaction of noble metal ions becomes mass transfer-limited. As a result, the whiskers grow from the aggregated particles on the surface, and the large concentration gradient of metal ions from the bulk to the surface induces the metal ions to easily be reduced at the edge of the whiskers where the concentration of metal ions is much higher

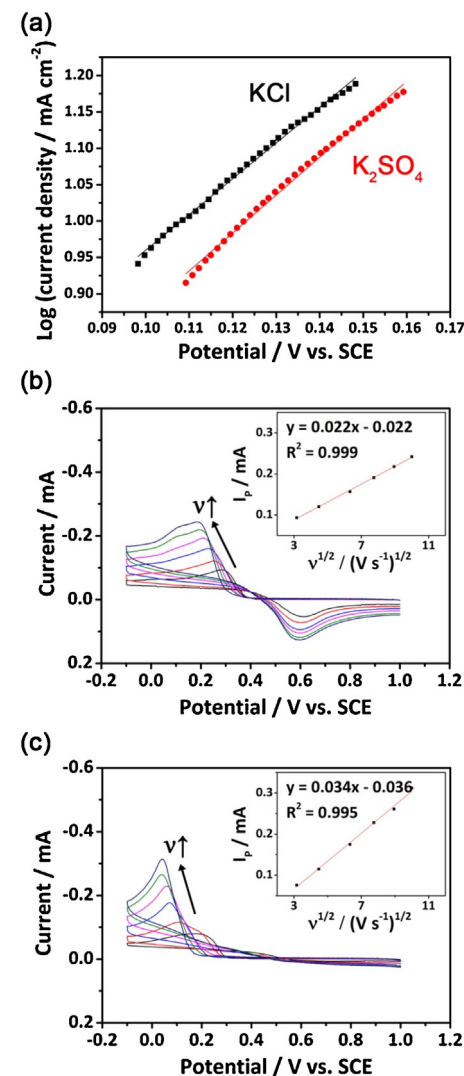


**Fig. 4.** (a) Tafel plots of Cu substrate in 6 mM KCl and 3 mM  $\text{K}_2\text{SO}_4$  aqueous solutions and the cyclic voltammograms of glassy carbon electrode in 0.1 M  $\text{HClO}_4$  aqueous solutions with (b) 3 mM  $\text{PdCl}_2$  and (c) 3 mM  $\text{PdSO}_4$  at the sweeping rates ( $v$ ) between 10 and 100  $\text{mV s}^{-1}$ . Insets are linear relationship between peak current ( $I_p$ ) and sweep rate ( $v^{1/2}$ ).

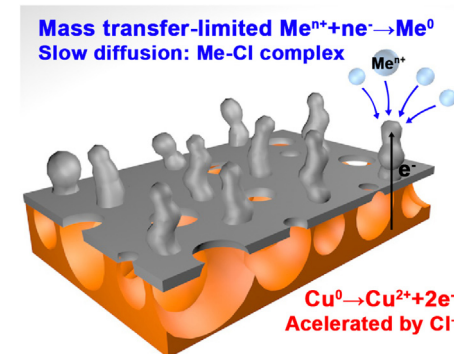


**Fig. 5.** Schematic diagram for the mechanism of whisker formation during galvanic displacement.

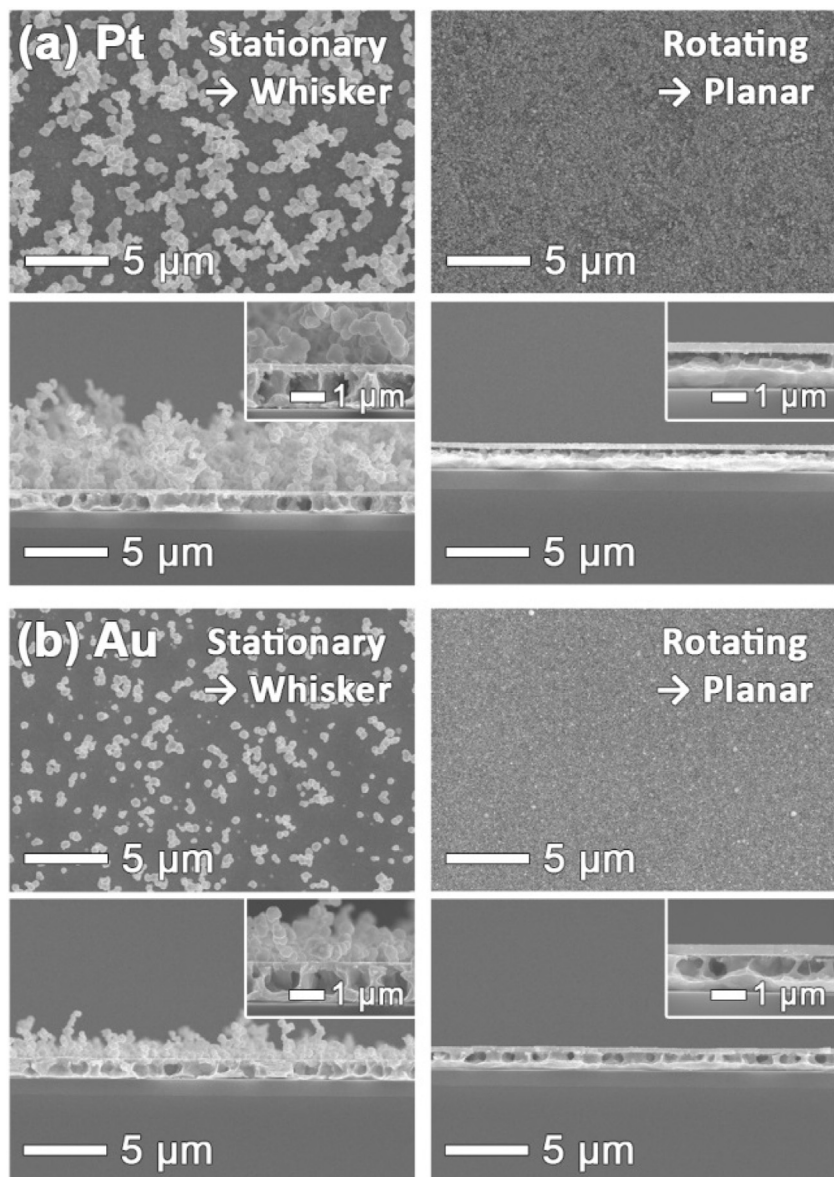


**Fig. 6.** Surface and cross-sectional images of (a) Pt and (b) Au deposits prepared by galvanic displacement in  $\text{K}_2\text{PtCl}_4$  and  $\text{AuCl}_3$  solutions, respectively. The substrates remained stationary for 30 min or rotating at 300 rpm for 2 min during the reaction.

than that on the surface of substrate. On the contrary, when the development of the concentration gradient is suppressed by rotating the substrate or using  $\text{SO}_4^{2-}$ , relatively high concentration of metal ion remains near the substrate surface. As a result, the planar catalysts form on the substrate instead of whisker shape as shown in Fig. 1(b) and (c).

Previously, it has been reported that the formation of Ag dendrites was induced by the diffusion-limited condition with oriented attachment and was followed by reorientation of Ag aggregates at the edge of dendrites [34–36]. The surface energy-driven attachment and reorientation led to the fractal growth of Ag with a 50–60° difference between the growth directions of backbone and branches, which supported that the surface energy played an important role in driving the fractal growth of Ag. However, the fractal growth of Pd was not observed for the conditions examined in this study, meaning that the surface energy is not a decisive factor to form whisker-type Pd.

The validity of the suggested displacement method for whisker formation was confirmed with Pt and Au (Fig. 6). Whisker forma-

tion during galvanic displacement was ascribed to development of a concentration gradient. Therefore, Pt and Au displacement was conducted using a metal precursor containing  $\text{Cl}^-$  with and without rotating the substrate. As expected, in the absence of rotation, whisker-type Pt and Au were evident, together with large cavities within the Cu substrate. In contrast, flat and smooth Pt and Au were deposited with substrate rotation. These results suggest that this galvanic displacement method of controlling the surface morphology is not limited by the kind of metal to be deposited.

### 3.3. Characteristics and electrocatalytic performance of Pd whisker

The characteristics of whisker-type Pd deposit and its electrocatalytic performance towards ethanol oxidation were investigated. Whisker and planar deposits were prepared by the conditions used for Fig. 1. Pd and Cu distributions after displacement are shown in Fig. 7(a). The EDS line-scan and mapping for whisker indicate that the whisker contained a markedly higher Pd

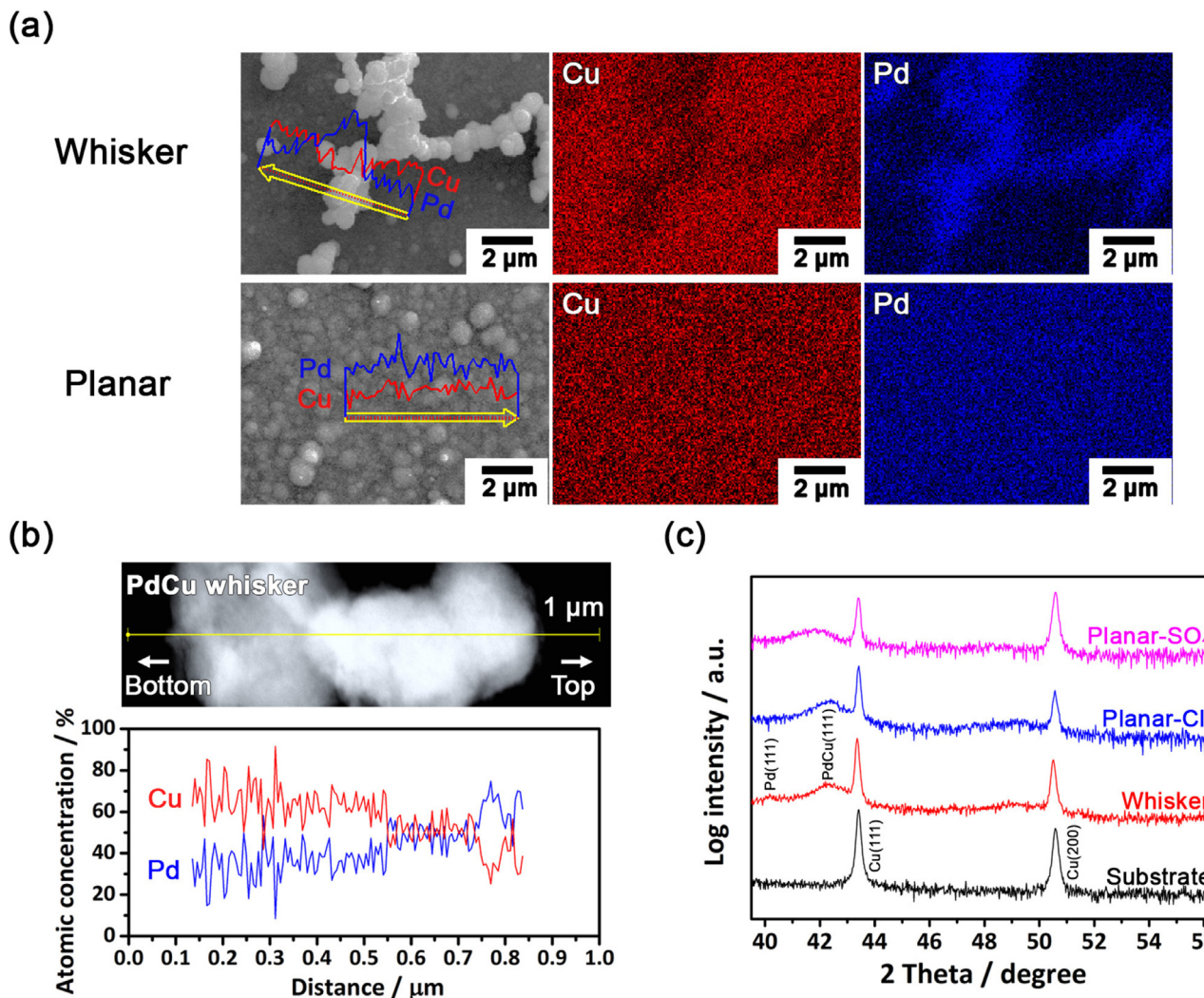


**Fig. 7.** (a) FE-SEM with EDS line-scan and corresponding EDS mapping images of whisker and planar Pd (Planar-Cl<sup>-</sup>) deposits, (b) TEM image of a whisker with corresponding line profiles of elemental composition by EDS along the yellow line, and (c) XRD patterns of pristine Cu substrate, whisker, and planar samples. The planar Pd layers were obtained from PdCl<sub>2</sub> solution with rotation of the substrate (Planar-Cl<sup>-</sup>) and PdSO<sub>4</sub> solution without rotation (Planar-SO<sub>4</sub><sup>2-</sup>). (For interpretation of the references to colour in this figure legend, the reader is referred to the web version of this article.)

content than the surrounding planar region. The mapping result suggests that most Pd ions, moving from the bulk solution to the surface of substrate, contributed to whisker formation. In comparison, Pd was uniformly distributed in the planar sample. In addition, as shown in Fig. 7(b), the TEM/EDS line-scan of a whisker in the vertical direction indicated that the whisker consisted of PdCu alloy and the Pd concentration increased from the bottom to the top of the whisker. Notably, the Cu ions produced by substrate dissolution could be co-deposited with Pd. The atomic concentration of Cu decreased from bottom to top, since dissolved Cu ions remaining near the surface were easily re-deposited at the bottom. The EDS results in Fig. 7(a) and (b) indicate that Pd ions reaching the surface contributed to whisker growth in the absence of agitation. Fig. 7(c) shows the XRD patterns of whisker and planar samples, which also supported Pd-Cu co-deposition. Diffraction peaks corresponding to PdCu(111) were evident between 41° and 43° of two-theta, corresponding to pure Pd(111) and Cu(111), regardless of deposit structure. In addition, the d-spacing of adjacent lattice fringes of the whisker is 0.218 nm (Fig. S4) which is between the lattice distances of pure Pd (0.224 nm) and Cu (0.208 nm), meaning that Pd-Cu was co-deposited during galvanic displacement [37,38]. In addition, it was found that the surfaces of two planar Pd-Cu films

from PdCl<sub>2</sub> and PdSO<sub>4</sub> solutions were composed of 15 at% Pd-85 at% Cu and 53 at% Pd-47 at% Cu, respectively (Fig. S5). The method to calculate the atomic ratio is presented in Supporting Information.

The galvanic displacement of Pt and Au (Fig. 6) also resulted in the formation of their alloys with Cu regardless of the morphology. XRD patterns for displaced Pt and Au are shown in Fig. S6, indicating that there were small peaks between pure Pt and Cu, and between pure Au and Cu. Furthermore, Pt and Au whiskers contained considerable amounts of Cu as shown in Fig. S7. Interestingly, Cu content in Pt whisker was much higher as compared to Pd and Au whiskers. In addition, the surfaces of the planar Pt-Cu and Au-Cu films were composed of 25 at% Pt-75 at% Cu and 14 at% Au-86 at% Cu calculated from XPS spectra (Fig. S8). The mechanism of alloy formation during galvanic displacement and the way to control the composition of alloy should be further investigated.

The electrochemically active surface area and the electrochemical performance of the Pd-Cu whisker for ethanol oxidation were further investigated. The electrochemically active surface area of Pd disk and whisker electrodes was calculated by integrating the charges of Pd oxide reduction from the cyclic voltammogram shown in Fig. 8(a), assuming the charge for the reduction of Pd oxide monolayer to be 405  $\mu\text{C cm}^{-2}$  (calculation method shown in Sup-

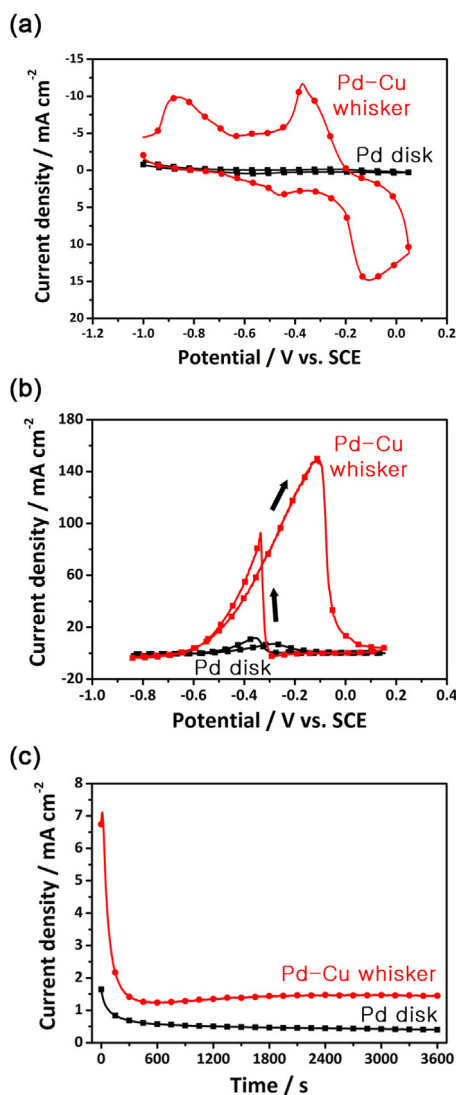


**Fig. 8.** Cyclic voltammograms of Pd–Cu whisker and Pd disk electrodes (a) in 0.5 M KOH solution with a scan rate of 50 mV s<sup>-1</sup> and (b) 1 M KOH and 1 M ethanol solution with a scan rate of 20 mV s<sup>-1</sup>. (c) i–t curves of Pd–Cu whisker and Pd disk electrodes in 1 M KOH and 1 M ethanol solution at -0.245 V for 3600 s.

porting Information) [39]. The surface areas of Pd disk and Pd–Cu whisker electrodes were 0.241 cm<sup>2</sup> and 10.595 cm<sup>2</sup>, respectively, indicating that the whisker catalyst exhibited a 44-fold greater surface area for the electrochemical reaction than the planar catalyst. Fig. 8(b) shows the cyclic voltammograms of the Pd–Cu whisker and Pd disk electrodes for ethanol oxidation reaction, associated with direct ethanol fuel cells (DEFCs) [40,41]. Two oxidation current peaks appear in forward and reverse scans. In the forward scan, the oxidation peak located at -0.3 V is assigned to the oxidation of freshly chemisorbed ethanol. Whereas, the oxidation peak in the reverse scan located at -0.4 V is associated with the removal of carbonaceous species not completely oxidized in the forward scan [40]. The current density of oxidation peak in the forward scan for Pd–Cu whisker (146.5 mA cm<sup>-2</sup>) is 21-fold higher compared to Pd disk (7.0 mA cm<sup>-2</sup>). The peak current densities for planar Pd–Cu obtained from PdCl<sub>2</sub> (with rotating) and PdSO<sub>4</sub> (without rotating) solutions were 22.8 and 19.1 mA cm<sup>-2</sup>, respectively (Fig. S11). The peak current densities normalized by the amount of Pd loading were 491.2, 69.7, and 113.0 mA cm<sup>-2</sup> μg<sup>-1</sup> for Pd–Cu whisker (0.298 μg of Pd), and planar Pd–Cu from PdCl<sub>2</sub> (0.327 μg) and PdSO<sub>4</sub> (0.169 μg) solutions, respectively. It was obvious that whisker-type

catalyst is the most active and cost-effective for ethanol oxidation. The onset potential for the ethanol oxidation on the Pd–Cu whisker electrode is -0.65 V, which is more negative than -0.56 V from Pd disk. As shown in Fig. S11, the onset potentials for planar Pd–Cu from PdCl<sub>2</sub> and PdSO<sub>4</sub> solutions were -0.62 V and -0.61 V, respectively. Regardless of the morphology, the onset potential for ethanol oxidation was negatively shifted, implying the improvement in the catalytic activity for the ethanol oxidation reaction over Pd disk electrode. As confirmed by XRD and TEM/EDS analyses, the Pd displacement for the conditions examined in this study resulted in the alloy formation. The improvement in the electrocatalytic activity observed in Figs. 8(b) and S11 is also obtained from the synergetic effect by the interaction between Pd and Cu in their alloys [40,41]. In the case of whisker, the content of Pd varied with the height of whisker, thus it is hard to directly compare the effect of alloy composition on the catalytic activity for ethanol oxidation. On the contrary, the catalytic activities of planar Pd–Cu prepared from PdCl<sub>2</sub> and PdSO<sub>4</sub> solutions could be explained based on the content of Pd. It was previously reported that Pd alloyed with Cu showed better catalytic activity than pure Pd and the atomic concentration of Pd showing the best electrocatalytic activity was 50 at% [42]. Therefore, planar Pd–Cu with more Pd (53 at% of Pd) from PdSO<sub>4</sub> solution showed higher electrocatalytic activity than that from PdCl<sub>2</sub> solution (15 at% of Pd) as calculated from Fig. S5. The stabilities of disk and whiskered electrodes were finally investigated by chronoamperometry at the potential of -0.245 V for 3600 s (Fig. 8(c)), and it was obvious that Pd–Cu whisker has better electrocatalytic performance towards ethanol oxidation than Pd disk in long-term.

#### 4. Conclusions

We have demonstrated a one-step galvanic displacement method to control the morphology of noble metal deposits. The alteration of the rates of oxidation reaction and metal ion mass transfer during galvanic displacement facilitated modification of the structure of noble metal deposits. The steep concentration gradient of metal ion was essential for fabricating whisker-type metal deposits. This method can be applied to the fabrication of catalysts comprising various noble metals – including Pd, Pt, and Au – with a dramatic increase in the surface areas. It was also confirmed that the whisker-type Pd catalyst had superior electrocatalytic performance than planar catalyst. Therefore, we suggest that this galvanic displacement method for controlling the morphology of metal deposits can be applied to various electrocatalytic systems to improve the electrochemical performance.

#### Acknowledgments

This work was supported by the “R&D Center for reduction of Non-CO<sub>2</sub> Greenhouse gases (2013001690004)” funded by the Korea Ministry of Environment (MOE) as “Global Top Environment R&D Program”.

#### Appendix A. Supplementary data

Supplementary data associated with this article can be found, in the online version, at <http://dx.doi.org/10.1016/j.apcatb.2017.05.094>.

#### References

- [1] A. Mohanty, N. Garg, R. Jin, A universal approach to the synthesis of noble metal nanodendrites and their catalytic properties, *Angew. Chem. Int. Ed.* **49** (2010) 4962–4966.
- [2] M. Shao, K. Sasaki, N.S. Marinkovic, L. Zhang, R.R. Adzic, Synthesis and characterization of platinum monolayer oxygen-reduction electrocatalysts

with Co–Pd core–shell nanoparticle supports, *Electrochem. Commun.* 9 (2007) 2848–2853.

[3] A. Sarkar, A. Manthiram, Synthesis of Pt@Cu core–shell nanoparticles by galvanic displacement of Cu by Pt<sup>4+</sup> ions and their application as electrocatalysts for oxygen reduction reaction in fuel cells, *J. Phys. Chem. C* 114 (2010) 4725–4732.

[4] C. Koenigsmann, A.C. Santulli, K. Gong, M.B. Vukmirovic, W.-p. Zhou, E. Sutter, S.S. Wong, R.R. Adzic, Enhanced electrocatalytic performance of processed, ultrathin, supported Pd–Pt core–shell nanowire catalysts for the oxygen reduction reaction, *J. Am. Chem. Soc.* 133 (2011) 9783–9795.

[5] Y.G. Guo, J.S. Hu, H.M. Zhang, H.P. Liang, L.J. Wan, C.L. Bai, Tin/platinum bimetallic nanotube array and its electrocatalytic activity for methanol oxidation, *Adv. Mater.* 17 (2005) 746–750.

[6] K.H. Kim, T. Lim, M.J. Kim, S. Choe, S. Baek, J.J. Kim, Porous indium electrode with large surface area for effective electroreduction of N<sub>2</sub>O, *Electrochem. Commun.* 62 (2016) 13–16.

[7] Y. Gauthier, M. Schmid, S. Padovani, E. Lundgren, V. Buš, G. Kresse, J. Redinger, P. Varga, Adsorption sites and ligand effect for CO on an alloy surface: a direct view, *Phys. Rev. Lett.* 87 (2001) 036103.

[8] J.K. Nørskov, F. Abild-Pedersen, F. Studt, T. Bligaard, Density functional theory in surface chemistry and catalysis, *Proc. Natl. Acad. Sci. U. S. A.* 108 (2011) 937–943.

[9] W. Zhang, F. Tan, W. Wang, X. Qiu, X. Qiao, J. Chen, Facile:template-free synthesis of silver nanodendrites with high catalytic activity for the reduction of p-nitrophenol, *J. Hazard. Mater.* 217 (2012) 36–42.

[10] W. Lee, R. Ji, U. Gösele, K. Nielsch, Fast fabrication of long-range ordered porous alumina membranes by hard anodization, *Nature Mater.* 5 (2006) 741–747.

[11] Y. Sun, Y. Wang, Monitoring of galvanic replacement reaction between silver nanowires and HAuCl<sub>4</sub> by in situ transmission X-ray microscopy, *Nano Lett.* 11 (2011) 4386–4392.

[12] H. Li, C. Liang, M. Liu, K. Zhong, Y. Tong, P. Liu, G.A. Hope, Synthesis of indium nanowires by galvanic displacement and their optical properties, *Nanoscale Res. Lett.* 4 (2009) 47–53.

[13] Y. Wang, M. Becker, L. Wang, J. Liu, R. Scholz, J. Peng, U. Gösele, S. Christiansen, D.H. Kim, M. Steinhart, Nanostructured gold films for SERS by block copolymer-templated galvanic displacement reactions, *Nano Lett.* 9 (2009) 2384–2389.

[14] S.M. Alia, G. Zhang, D. Kisailus, D. Li, S. Gu, K. Jensen, Y. Yan, Porous platinum nanotubes for oxygen reduction and methanol oxidation reactions, *Adv. Funct. Mater.* 20 (2010) 3742–3746.

[15] H. Zhang, M. Jin, H. Liu, J. Wang, M.J. Kim, D. Yang, Z. Xie, J. Liu, Y. Xia, Facile synthesis of Pd–Pt alloy nanocages and their enhanced performance for preferential oxidation of CO in excess hydrogen, *ACS Nano* 5 (2011) 8212–8222.

[16] C.M. Cobley, Y. Xia, Engineering the properties of metal nanostructures via galvanic replacement reactions, *Mater. Sci. Eng. R-Rep.* 70 (2010) 44–62.

[17] I. Choi, S.H. Ahn, J.J. Kim, O.J. Kwon, Preparation of P shell–Pd core nanoparticle with electroless deposition of copper for polymer electrolyte membrane fuel cell, *Appl. Catal. B: Environ.* 102 (2011) 608–613.

[18] N. Travitsky, T. Ripenbein, D. Golodnitsky, Y. Rosenberg, L. Burshtein, E. Peled, PtNi- and PtCo-supported catalysts for oxygen reduction in PEM fuel cells, *J. Power Sources* 161 (2006) 782–789.

[19] S.-M. Hwang, J.E. Bonevich, J.J. Kim, T.P. Moffat, Formic acid oxidation on Pt<sub>100-x</sub>Pb<sub>x</sub> thin films electrodeposited on Au, *J. Electrochem. Soc.* 158 (2011) B1019–B1028.

[20] R. Jayashree, J. Spendelow, J. Yeom, C. Rastogi, M. Shannon, P. Kenis, Characterization and application of electrodeposited PtPt/Pd, and Pd catalyst structures for direct formic acid micro fuel cells, *Electrochim. Acta* 50 (2005) 4674–4682.

[21] A. Sharma, M. Suresh, H. Bhojraj, H. Narayananamurthy, R. Sahu, Electroless nickel plating on magnesium alloy, *Met. Finish.* 96 (1998) 10–16.

[22] M. Tortosa, M. Mollar, B. Mari, Synthesis of ZnCdO thin films by electrodeposition, *J. Cryst. Growth* 304 (2007) 97–102.

[23] L. Au, X. Lu, Y. Xia, A comparative study of galvanic replacement reactions involving Ag nanocubes and AuCl<sub>2</sub><sup>–</sup> or AuCl<sub>4</sub><sup>–</sup>, *Adv. Mater. (Deerfield Beach Fla.)* 20 (2008) 2517–2522.

[24] D.-Y. Park, H. Jung, Y. Rheem, C. Hangarter, Y.-I. Lee, J. Ko, Y.-H. Choa, N. Myung, Morphology controlled 1D Pt nanostructures synthesized by galvanic displacement of Cu nanowires in chloroplatinic acid, *Electrochim. Acta* 55 (2010) 4212–4216.

[25] L. Magagnin, R. Maboudian, C. Carraro, Gold deposition by galvanic displacement on semiconductor surfaces: effect of substrate on adhesion, *J. Phys. Chem. B* 106 (2002) 401–407.

[26] L.A. Porter, H.C. Choi, A.E. Ribbe, J.M. Buriak, Controlled electroless deposition of noble metal nanoparticle films on germanium surfaces, *Nano Lett.* 2 (2002) 1067–1071.

[27] M.H. Shao, T. Huang, P. Liu, J. Zhang, K. Sasaki, M.B. Vukmirovic, R.R. Adzic, Palladium monolayer and palladium alloy electrocatalysts for oxygen reduction, *Langmuir* 22 (2006) 10409–10415.

[28] O. Ghodbane, L. Roué, D. Bélanger, Study of the electroless deposition of Pd on Cu-Modified graphite, *Chem. Mater.* 20 (2008) 3495–3504.

[29] J.G. Song, G.H. Ryu, S.J. Lee, S. Sim, C.W. Lee, T. Choi, H. Jung, Y. Kim, Z. Lee, J.M. Myoung, C. Dussarrat, C. Lansalot-Matras, J. Park, H. Choi, H. Kim, Controllable synthesis of molybdenum tungsten disulfide alloy for vertically composition-controlled multilayer, *Nat. Commun.* 6 (2015) 7817.

[30] X. Zhang, W. Wang, J. Liu, S. Sheng, G. Xiong, W. Yang, Hydrogen transport through thin palladium–copper alloy composite membranes at low temperatures, *Thin Solid Films* 516 (2008) 1849–1856.

[31] B. Kim, T. Ritzdorf, Electrodeposition of near-eutectic SnAg solders for wafer-level packaging, *J. Electrochem. Soc.* 150 (2003) C577–C584.

[32] H. Otmačić, J. Telegdi, K. Papp, E. Stupnišek-Lisac, Protective properties of an inhibitor layer formed on copper in neutral chloride solution, *J. Appl. Electrochem.* 34 (2004) 545–550.

[33] S. Kaja, S.P. Mukherjee, E.J. O'sullivan, M. Paunovic, Palladium sulfate solution for the selective seeding of the metal interconnections on polyimide dielectrics for electroless metal deposition, In Google Patents, 1995.

[34] J. Fang, H. You, P. Kong, Y. Yi, X. Song, B. Ding, Dendritic silver nanostructure growth and evolution in replacement reaction, *Cryst. Growth Des.* 7 (2007) 864–867.

[35] S. Xie, X. Zhang, D. Xiao, M.C. Paau, J. Huang, M.M.F. Choi, Fast growth synthesis of silver dendrite crystals assisted by sulfate ion and its application for surface-enhanced Raman scattering, *J. Phys. Chem. C* 115 (2011) 9943–9951.

[36] J. Fang, H. You, C. Zhu, P. Kong, M. Shi, X. Song, B. Ding, Thermodynamic and kinetic competition in silver dendrite growth, *Chem. Phys. Lett.* 439 (2007) 204–208.

[37] Y. Wang, B. Liu, S. Xiao, H. Li, L. Wang, D. Cai, D. Wang, Y. Liu, Q. Li, T. Wang, High performance and negative temperature coefficient of low temperature hydrogen gas sensors using palladium decorated tungsten oxide, *J. Mater. Chem. A* 3 (2015) 1317–1324.

[38] T. Gao, G.W. Meng, J. Zhang, Y.W. Wang, C.H. Liang, J.C. Fan, L.D. Zhang, Template synthesis of single-crystal Cu nanowire arrays by electrodeposition, *Appl. Phys. A* 73 (2001) 251–254.

[39] Z.-Y. Shih, C.-W. Wang, G. Xu, H.-T. Chang, Porous palladium copper nanoparticles for the electrocatalytic oxidation of methanol in direct methanol fuel cells, *J. Mater. Chem. A* 1 (2013) 4773–4778.

[40] J. Liu, Z. Huang, K. Cai, H. Zhang, Z. Lu, T. Li, Y. Zuo, H. Han, Clean synthesis of an economical 3D nanochain network of PdCu alloy with enhanced electrocatalytic performance towards ethanol oxidation, *Chem. Eur. J.* 21 (2015) 17779–17785.

[41] C. Hu, X. Zhai, Y. Zhao, K. Bian, J. Zhang, L. Qu, H. Zhang, L. Hongxia, Small-sized PdCu nanocapsules on 3D graphene for high-performance ethanol oxidation, *Nanoscale* 6 (2014) 2768–2775.

[42] A. Serov, T. Asset, M. Padilla, I. Matanovic, U. Martinez, A. Roy, K. Artyushkova, M. Chatenet, F. Maillard, D. Bayer, C. Cremers, Highly-active Pd–Cu electrocatalysts for oxidation of ubiquitous oxygenated fuels, *Appl. Catal. B* 191 (2016) 76–85.